Multi-level Lagrangian analysis of the northern stratospheric polar vortex split in April 2020

J. Curbelo[1], G. Chen[2], and C. R. Mechoso[2]

[1]Departament de Matemàtiques, Universitat Politècnica de Catalunya, Barcelona, Spain
[2]Department of Atmospheric and Oceanic Sciences, University of California, Los Angeles, CA, USA

Key Points:

- Lagrangian structures with polar hyperbolic trajectories are identified in the vortex split.
- Trajectory analysis indicates ozone poor air remains in the main vortex at split.
- Split is linked to strong synoptic scale disturbances in the troposphere.

Corresponding author: Jezabel Curbelo, jezabel.curbelo@upc.edu

Abstract

The present paper examines the northern stratosphere during April 2020, when the polar vortex split into two cyclonic vortices after a winter with the strongest ozone depletion on record. We examine the dynamical evolution that led to the split at middle and lower stratospheric levels and the distribution of ozone between the main and off-spring vortices. Finally, we look at the vertical structure of the split down to the troposphere. The split event is analyzed with Lagrangian tools and an Eulerian diagnostic of planetary wave activity. The findings confirm the key role for the split played by a flow configuration with a polar hyperbolic trajectory and associated manifolds. A trajectory analysis illustrates how the ozone distribution between vortices was such that ozone poor air remained in the main vortex. The off-spring vortex became part of a deep structure from the troposphere, and connections with tropospheric disturbances over Eurasia are suggested.

Plain Language Summary

The Northern Hemisphere stratosphere during winter and early spring of 2020 had multiple outstanding features. Winter showed the strongest ozone depletion on record for the hemisphere accompanied by very low temperatures. The subsequent stratospheric evolution was punctuated by dramatic events, which included an episode of polar warming at upper levels in March and the split of the polar vortex into two cyclonic vortices at middle and lower levels in mid April. A remarkable mass of ozone poor air persisted within the westerly circulation throughout the period which also split with the polar vortex. We search for the answer to several outstanding questions in stratospheric dynamics and tracer evolution: What flow structures lead to the vortex split? How were air parcels with different ozone concentrations distributed between the vortices during the split? How were these events connected to tropospheric events? Our approach is based on following parcels trajectories, examining barriers to the tracer transport, and diagnosing the activity and propagation of planetary waves. We highlight the special polar configuration associated with stratospheric vortex splits. Our trajectory analysis illustrates the transport of ozone between the vortices during the split. We also look into associations between the split and strong perturbations in the troposphere.

1 Introduction

The Northern Hemisphere stratosphere during late winter and early spring of 2020 was remarkable in several ways. The polar night vortex was strong and persistent from December to February, consistent with the fact that the wave activity input from the troposphere was low and the Arctic Oscillation was in an unprecedentedly strong positive phase (Lawrence et al., 2020; Lee et al., 2020; Hardiman et al., 2020). The lowest values of stratospheric ozone on record were observed during the period (Manney et al., 2020; Wohltmann et al., 2020) and the Arctic ultraviolet radiation was unusually high at the surface (Bernhard et al., 2020). The subsequent evolution of the stratospheric flow showed dramatic dynamical events. These included around mid-March a warming amounting to tens of Kelvin of the polar region in the upper stratosphere. Around 22 April, the cyclonic vortex of the polar night split and there were two cyclonic vortices from the upper troposphere to the middle stratosphere. We will refer to the vortex that developed over North America as the "offspring" of the "main" vortex over northern Eurasia. These two vortices remained clearly identifiable for a few days, interacting with each other although the lowest ozone mixing ratio (O_3) remained within the main one. Afterwards, the westerly circulation weakened following the seasonal evolution to summer conditions. These outstanding and relatively rare dynamics and tracer events raise a number of questions. What dynamical processes lead to the mid-April split of the westerly polar vortex at middle levels? What types of interactions occurred between the two resulting vortices such that the lowest O_3 values remained within one of them? April 2020 also saw strong dynamical events in the troposphere. A strong ridge developed south

of Alaska (Lawrence et al., 2020) accompanied by a deep low over North America in a period of warm sea surface temperature anomalies in the eastern equatorial Pacific. One would wonder if the stratospheric events mentioned above were connected to tropospheric events. In a broader context, we aim to verify whether the dynamical structure of the split followed the mechanism we suggested in a previous case study, and to gain insight on whether in split cases the parcels in the off-spring vortex come from preferred locations (such as the periphery) of the main vortex.

The main focus of the present paper is on the development of the vortex split in April 2020 and associated features in the ozone distributions. Large geometrical distortions of the vortex lead to large equatorward displacements of vortex air that influence the column ozone and distribution of surface UV in populated regions. The period and issues we aim to examine provide a suitable case for a Lagrangian analysis of the evolving flow in the stratosphere. Lagrangian techniques allow to carry out a detailed study of the complicated dynamics of vortex split events and show how it impacts transport. Manney et al. (2015) and Manney and Lawrence (2016) used Lagrangian tools to examine polar vortex splits from the perspective of polar chemical processing and ozone depletion. The former authors showed that the major sudden warming of the split-type in 2012/2013 briefly enhanced ozone loss. The latter authors examined the Arctic polar vortex in the 2015/2016 winter, which was also persistently strong and cold and it was cut short because of an early final warming which occurred in the beginning of March. This warming and following vortex split in mid-March, did not lead to a significant stratospheric ozone deficit. Our Lagrangian tools will be those that we have used to analyze the unique vortex split event in the southern stratosphere during the final warming of 2002 (Curbelo et al., 2019b, 2019a; García-Garrido et al., 2017). To explore stratosphere-troposphere links we will use Eulerian diagnostics of wave activity and its propagation following Plumb (1985).

We start in section 2 with a description of data and methods including the Lagrangian tools used. Section 3 is a multi-level description of the flow with an emphasis on the period from 10 April to the vortex split on 22 April. Section 4 examines the distribution of fluid parcels between the vortices resulting from the split. Section 5 briefly discusses connections with the troposphere. Our conclusions are presented in section 6.

2 Data and methods

We use data from ERA5, the fifth generation ECMWF atmospheric reanalysis of the global climate Copernicus Climate Change Service (C3C) (Hersbach et al., 2018). The data provides wind velocity $[ms^{-1}]$, geopotential $[m^2s^{-2}]$, potential vorticity $[Km^2kg^{-1}s^{-1}]$ and O_3 $[kgkg^{-1}]$. The spatial resolution of the data we analyze is 0.25° lon. $\times$ 0.25° lat. with 37 pressure levels. The temporal resolution of the data is one hour, which is the highest available in the dataset.

Our Lagrangian descriptor of choice is the function M (Mancho et al., 2013). This is defined by the expression,

$$M(\mathbf{x}_0, t_0, \tau) = \int_{t_0-\tau}^{t_0+\tau} \|\mathbf{v}(\mathbf{x}(t;\mathbf{x}_0), t)\| \, dt \, , \tag{1}$$

where $\mathbf{v}(\mathbf{x}, t)$ is the two-dimensional (2D) velocity field on isentropic surfaces and $\|\cdot\|$ denotes Euclidean norm. Geometrically, a fluid parcel located at x_0 at time $t = t_0$ travels a length M during the period from $(t_0 - \tau)$ to $(t_0 + \tau)$. Our calculation of trajectories is carried out in a cartesian coordinate system to avoid issues at the pole, and uses a Cash - Karp Runge-Kutta scheme for advancing in time. The reader is referred to Curbelo et al. (2017) and references therein for a full description of our methodology. In our calculations of M we use $\tau = 10$ days. The curves on isentropic surfaces where $\|\nabla M\|$, the euclidean norm of the horizontal gradient of M, has large magnitudes approximate manifolds that act as instantaneous flow barriers (Mancho et al., 2013). To represent manifolds we will take 0.7 as the threshold

value for the normalized $\|\nabla M\|$ over the entire northern hemisphere at the time of the plot. We determined by experimentation that this threshold value captures the features of the manifolds that we wish to highlight.The intersections of the curves corresponding to unstable and stable manifolds give the approximate locations of hyperbolic trajectories (HT) from (to) which parcel asymptotically approach (separate) at different times. We adopt this approximation because no objective method to determine HTs from a geophysical vector field is available to our knowledge.

M also provides a visualization of the (kinematic) vortex boundary that is helpful in transport studies. Curbelo et al. (2019b) employed arguments of ergodic theory to conjecture that, on either a horizontal or an isentropic surface, a contour of M for a value very close to its maximum on the surface would be such that, (i) it divides the Stratospheric Polar Vortex (SPV) core from its surroundings, and (ii) it is free of hyperbolic trajectories and hence tends to not produce filaments during a certain time interval. In a nutshell, regions with large values of M computed with sufficiently large values of τ represent barriers of the flow. On the basis of results from numerical experiments Curbelo et al. (2019b) suggested that the threshold for M normalized by its maximum at each level can be taken as the lower limit of the fat tail in its probability density function (PDF). In the present paper, therefore, we define the kinematic vortex boundary as the region where the normalized value of M at each level is in the upper 7%. Note that according to this definition, the vortex boundary becomes a three-dimensional region contained between one inner and one outer surface instead of the single surface defined by the usual criterion based on potential vorticity and its maximum gradient in latitude.

3 The vortex split in April 2020

We set the vortex split date on 22 April from inspection of the trajectories of parcels on the vortex boundary shown in Movie S3. Figure 1 presents the evolution of the flow in the 10-day period before the split in the form of snapshots of M, O_3, and temperature at the 530K isentropic surface. The plot of M on 10 April captures a well-defined (cyclonic) vortex primarily symmetric about the North Pole. This is associated with an HT around $(45°W, 45°N)$. Inspection of the Hovmöller diagrams at 50 hPa for the longest planetary waves ($\sim$ 530 K) (Fig. S1) shows that the latitude of this HT corresponds to the critical level for wave 1, which is traveling eastward at the time. The unstable manifold extends west from this HT and leaves a clear signature on the large O_3 values over North America. Although it is not as well defined, there is another HT near the outer periphery of the vortex at around $(135°W, 65°N)$. This HT is around the critical level for wave 2, which is also traveling eastward at the time. From this HT, a plume of large O_3 values extends over the northern Pacific. The O_3 plots also show how the manifolds enclose the region of very low values inside the vortex. The relationship between manifolds and temperatures is less direct, as temperature is not a conservative property. Nevertheless, larger O_3 values and warmer temperatures are found over northern North America and Pacific Ocean. The plot of M on 15 April shows clear changes from five days earlier. The vortex still flows around the pole, but its shape is more triangular as zonal wavenumber 3 has amplified (Fig. S1). The HTs detected on 10 April have rotated eastward and another one can be discerned around $(140°E, 50°N)$. The imprints of the HTs on O_3 and temperature are clearly visible in the plots of these quantities. The plots of all quantities change dramatically from 15 to 20 April. M reveals that the vortex has pinched between high centers over the Pacific and Atlantic Oceans with large equatorward displacements of vortex air over North America. Another HT has developed very near the pole in association with the amplification of zonal wavenumber 2 (see Fig. S1).The low O_3 values remain within the vortex while the higher temperatures are around this region.

The configuration of the manifolds associated with the polar HT plays a key role in the vortex split. To visualize this key role we must look jointly in Fig. 1 at the three plots in the bottom row that correspond to 20 April, i.e. just 2 days before the split. For a conceptual

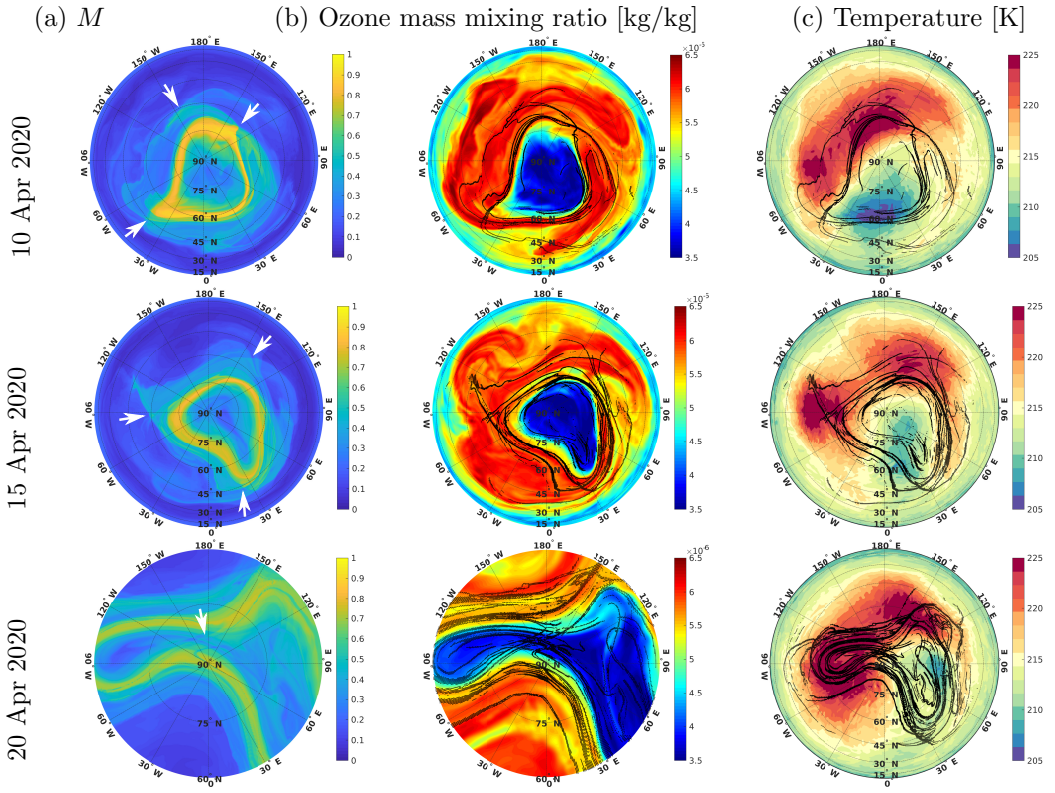

Figure 1. Maps at the 530K isentropic surface of the normalized Lagrangian descriptor M (column a), ozone mass mixing ratio [kg/kg] (column b), and temperature [K] (column c) on 10 April 2020 (upper row), 15 April 2020 (middle row) and 20 April 2020 (bottom row). The maps cover the domain poleward of 10N, except for those of M and ozone mass mixing ratio in the bottom row, which cover the region poleward of 60N for a better view of the polar region, The integration intervals for M (see the definitions in Eq. 1) are 31 March 00:00:00 - 20 April 00:00:00, 5 - 25 April 00:00:00 and 10 - 30 April 00:00:00, respectively. The black lines correspond to large values of $\|\nabla M\|$ and thus highlight the singular features of the function M approximating the manifolds locations. White arrows mark the HT locations referenced in the text.

view the reader is referred to the schematics in Fig. S2, which was introduced in a previous paper Curbelo et al. (2019a). Fluid parcels traveling at higher speeds - as evidenced by the larger values of M - from the periphery of the vortex in the eastern hemisphere, to the periphery of the vortex in the western hemisphere first approach the polar hyperbolic point along the stable manifold and next move away from it along the unstable manifold. As the parcels return to the eastern hemisphere, their path to the polar hyperbolic point is obstructed by the manifolds that have formed ahead. For a while, some of the parcels keep circling around the vortex in the western hemisphere while others are able to reach the other vortex. The latter transfer was interrupted when the two vortices split on 22 April.

The behaviors described in the previous paragraph are further illustrated by the trajectories of parcels inside the vortex boundary at 530K in Fig. 2. Using the same notation as in Movie S3, this figure shows trajectories computed forward in time and colored either blue or red according to whether the initial locations are along the outside or inside edge of the boundary, i.e. equatorward or poleward of the max(M) contour at the selected level. Recall that the vortex boundary is defined by the contours where the value of M is in the upper 7% of its PDF, and thus the vortex boundary is an area than a single line. On 19

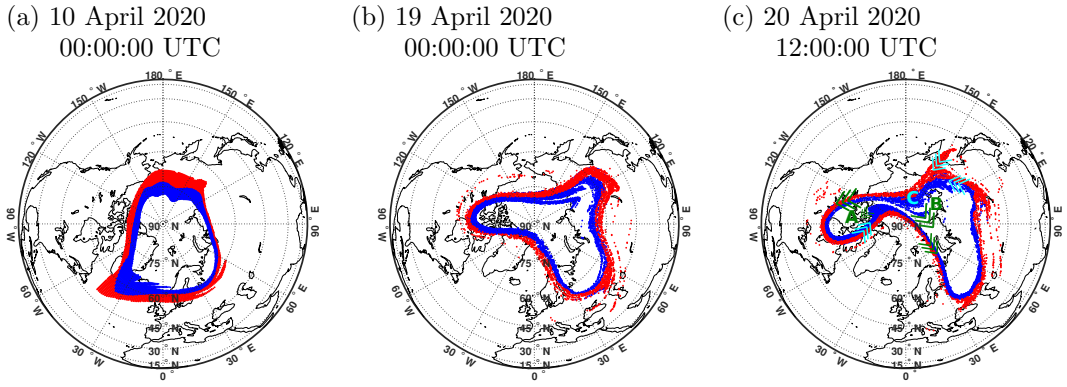

Figure 2. Panel (a) shows the locations of parcels at 530K on 10 April 2020 that are located between the contourlines corresponding to the 93th percentile of M at that level, using either blue or red to differentiate those that are inside or outside the contour defined by the maximum value of M at each longitude. Panels (b) and (c) indicate the horizontal locations of the parcels in (a) at different times approaching the SPV splitting. The directions of the parcels following the stable and unstable manifolds are shown in panel (c) with cyan and green arrows, respectively.

April the colored parcels surround the vortex, which is already considerably deformed. One day later, on 20 April at 12:00:00 UTC (Fig. 2(c)), the blue parcels in the subset labeled A are returning over northern North America to the vortex in the western hemisphere, in a configuration that strongly resembles the schematics in Fig. S2 (a). These parcels keep circling around the vortex in the eastern hemisphere while blue parcels in the subset C are still traveling to the other vortex. The vortex split is completed two days later, on 22 April, for which plots are presented in the next section.

4 Transfer of fluid parcels between the vortices during and after the split

In this section we look into how the transfer of fluid parcels between vortices occurred at 530K in mid-April 2020, and the extent to which O_3 behaved as an inert tracer. To address the first issue, we plot backward trajectories starting just around the split on 22 April when most parcels inside of the vortices are as identified by $O3$ values in the lower 10% for the level. The method of calculation of backwards trajectories is the same as the one used to compute M Moreover, we bin those parcels using either magenta or green color according the whether $O3$ is above and below 2%, respectively. Panels (a)-(d) of Fig. 3 show the locations at different times of the parcels colored using such scheme, and our narrative is organized as backwards in time. On 18 April, the set of parcels labeled with magenta color is very near the North Pole at both sides of the dateline and around the entire interior wall of the polar jet. On 15 April, these parcels are over Eurasia inside a U-shaped pattern formed by others with the lower ozone concentration in green. High ozone around vortex edge does not mix with vortex core ozone-depleted air despite the highly disturbed vortex event of mid-April. On 10 April, the configuration is broadly similar to the one 5 days later. The panels of Fig. 3 reveal that a set of parcels with higher $O3$ and within the vortex core on 10-15 April move counterclockwise along its inner boundary until they are transferred to the off-spring vortex in the western hemisphere. The panels also reveal that parcels with the lower O_3 values on 22 April did not transfer from the main vortex to the off-spring over North America. Movie S3 illustrates these parcels displacements with 1 hour resolution. The parcel transfer is such that the parcels with lowest O_3 remained in the main vortex. Also, a higher fraction of vortex edge air (red and blue parcels) ended up in the off spring vortex.

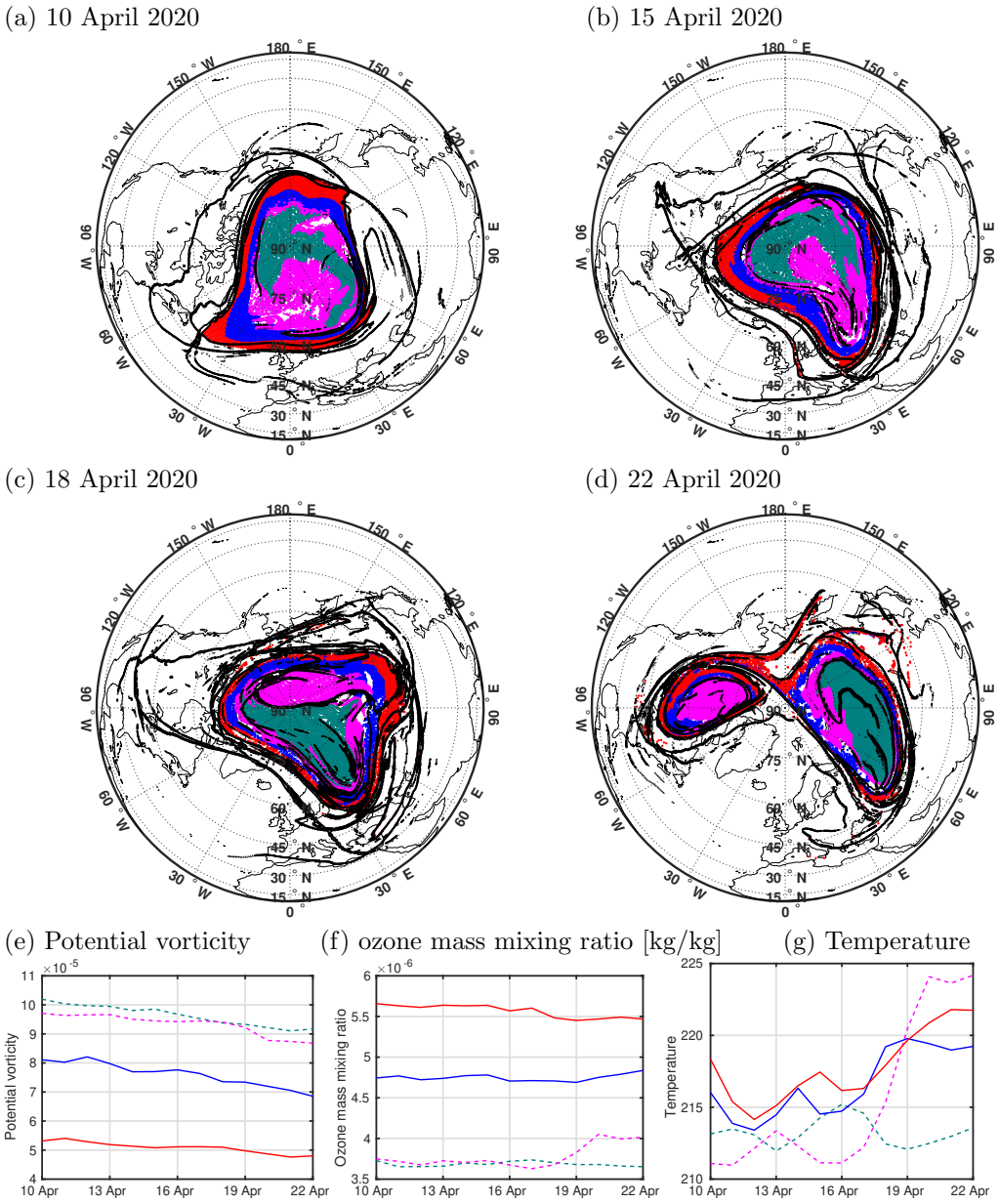

Figure 3. Panels (a)-(d) display backward parcel trajectories at 530K that are initialized on 22 April 2020. Magenta color identifies parcels that on 22 April, have O_3 values between the lower 10% and 2% for the level. Green color identifies parcels on 22 April have O_3 values in the lower 2% for the level. Blue and red color identifies the same parcels as in figure 2.In the panels, black lines correspond to large values of $\|\nabla M\|$, i.e. approximately the manifolds. M is calculated with $\tau = 10$ days, i.e. in an interval of 20 days centered on 10 April 00:00:00 (a), 15 April 00:00:00 (b), 18 April 00:00:00 (c), 22 April 00:00:00 (d). Panels (e)-(g) show the time series of mean potential vorticity, ozone mass mixing ratio, and temperature for the sets of parcels in green, magenta, red and blue. See the text for more information.

Panels (e), (f) and (g) of Fig. 3 show the time evolution of mean potential vorticity, O_3 and temperature respectively, for the different sets of parcels represented in panels (a)-(d) of the same figure with different colors. The time series of potential vorticity shows a

slightly decreasing trend. The values of O_3 (Fig. 3(f)) are relatively constant with a slight decreasing trend before April 20. The lowest ozone values are inside the vortex in the outer part (red line) of the vortex boundary is larger than in the inner part (blue line). This is in general agreement with the presence of an "ozone collar" around the vortex as reported by Mariotti et al. (2000) for the Antarctic polar vortex on the basis of airplane data. Fig. 3(g) shows a different behavior for temperature, without clear separations between the different colored regions. Note the temperature increase captured by the parcels inside the vortex with ozone concentration greater than 2% (magenta line) from 17 to 19 April, at which time the parcels with the lowest ozone concentration (< 2%) (green line) capture a decrease. The small range of potential vorticity and O_3 variations justifies the assumptions made about their approximate conservation during the study period. The temperature variations broadly agree with those expected from the split shown in the panels of Fig. 1.

5 Connections with the troposphere

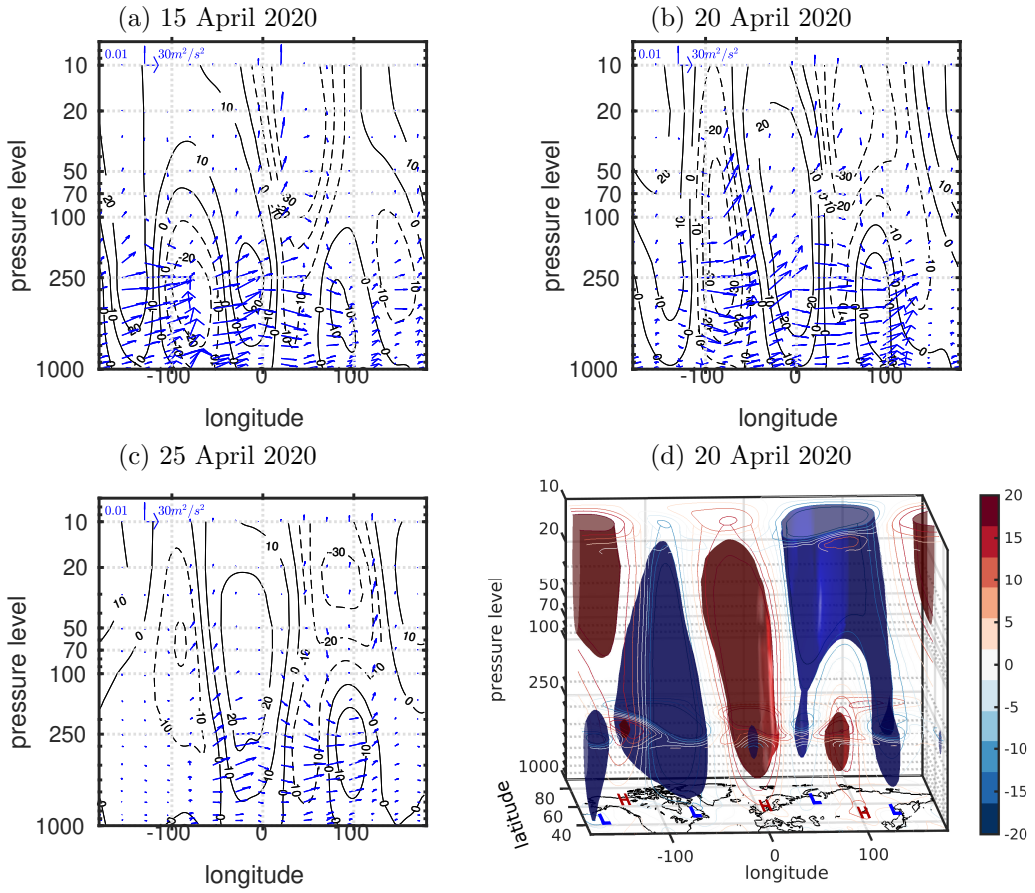

Figure 4. (a), (b), and (c) Averages between $55°N$-$65°N$ of QG stream function deviations from the zonal mean, and of wave activity flux F (Plumb, 1985) for 15, 20 and 25 April, respectively. Contour interval for QG is $10 \cdot 10^6 m^2/s$, positive solid and negative dashed. (d) 3D Isosurfaces of deviations of QG stream function from the zonal mean at values of -15·$10^6 m^2/s$ (blue) and 20·$10^6 m^2/s$(red). For added clarity, contour lines are drawn on the pressure surfaces at 1000hPa, 250hPa and 10hPa, as well as on the vertical surface at $65°N$. Latitude (degrees North), Longitude (degree East) and pressure level(hPa)

The QG stream function deviations from the zonal mean between $55°N$-$65°N$ are shown in Fig. 4 before and during the vortex pinching and after the two vortices have formed. The wave activity flux field is represented by F (Plumb, 1985) also averaged between the same latitude bands and for the same times. On 15 April, the negative stream function anomaly in panel (a) represents a cyclonic circulation centered over North America around $75°W$ extending up from 1000hPa. At the center of this circulation, the wave activity flux up to 250 hPa was upward. Another feature seen in panel (a) at upper levels is the vortex over northern Eurasia where the vertical wave activity flux is upward. Notice that at lower level under this vortex the vertical wave activity flux tends to be downward. The tropospheric disturbances are suggestive of a wave train from northern North America to northern Eurasia. On 20 April, the circulation centered over North America around $75°W$ reached levels above 10hPa, and the wave activity flux is strong and upward up to 50 hPa (see also Fig. 2). Other features on 20 April shown in panel (b) are essentially and amplification of those 5 days earlier. On 25 April, panel (c) shows the signature of zonal wavenumber 2 at upper levels, while the component of the tropospheric wave train below 100 hPa is still visible especially in the eastern hemisphere. These configurations of vertical wave activity flux suggests stratosphere-troposphere structures that were several kilometers deep. After the vortex split, on 25 April (panel (c)), the vertical wave activity flux decays in magnitude around $90°W$. Notably, F pointed slightly downward in the eastern hemisphere around $90°E$ suggests that the stratosphere may contribute to the tropospheric disturbances over northern Eurasia at this time as in the connections discussed by Kretschmer et al. (2018). Figure 4 (d) shows the isosurfaces of the QG stream function anomaly at value of -15·$10^6 m^2/s$ (blue) and 20·$10^6 m^2/s$ (red). Contour lines on the pressure surfaces at levels 1000hPa, 250hPa and 10hPa, as well as on the vertical surface at $65°N$, are shown in the same panel tor a pictorial view vertical structure of the circulations. Panel (d) in Fig. 4 illustrates the 3D structure of the circulations described by the vertical sections in panels (a), (b) and (c). The vortex over North America has a clearly defined troposphere-stratosphere structure, decreasing its size in height and closing at 30hPa. The deep vertical structure over North America and vertical wave activity flux are also consistent with the structures of intraseasonal variability in Guan et al. (2020), in which a stratospheric wave 1 pattern is associated a surface ridge over Alaska and a trough North America. Conversely, the vortex over Eurasia is better defined in the stratosphere.

6 Conclusions

We have examined dynamics and tracer transport occurring in the northern stratosphere around mid-April, when the main cyclonic vortex of the polar night displaced over northern Eurasia split and an off-spring cyclonic vortex developed above northern North America. The two vortices in remained distinct for a few days, after which they merged until the final warming was completed in mid-May. Our emphasis was placed on the split of the westerly polar vortex at middle stratospheric levels and on the interactions that occurred between the two vortices determining the resulting distribution of ozone. For the analysis we applied Lagrangian tools, including a Lagrangian descriptor, the estimation of HTs and associated manifolds, and a novel definition of the polar vortex boundary. We also used an Eulerian diagnostic of planetary wave activity and its propagation.

Inspection of the flow evolution prior to the vortex split revealed a configuration in which a polar hyperbolic trajectory (HT) plays a key role. Fluid parcels from the periphery of the vortex in the eastern hemisphere traveling at higher speeds towards near the HT along its stable manifold continue moving along the periphery of the vortex in the western hemisphere along the unstable manifold. As some of these parcels return to the eastern hemisphere, their path is obstructed by other developing manifolds and stay circling around the vortex in the western hemisphere while others are able to reach the other vortex. At some point in time, these transfer of fluid parcels were interrupted and the two vortices split. Such a behavior is similar to the one described in the vortex split during the final

warming of the southern stratosphere during spring of 2002 (Curbelo et al., 2019b). This finding reinforces the notion that the Lagrangian structures including a polar HT and special configuration of associated manifolds go beyond a single case study, and hence merits further investigation.

The evolutions described in the previous paragraph were illustrated by the field of parcel trajectories. Examination of this field further revealed that a set of parcels well within the vortex core on 10 April moved clockwise around the pole and along its inner boundary until these parcels transferred to the new vortex in the western hemisphere. Thus, the lower values of ozone were in the vortex interior over Eurasia on 22 April. Thus, in split cases the parcels in the off-spring vortex do not necessarily come from the periphery of the main vortex. This finding also merits further investigations as vortex interactions include transfer of fluid parcels, which may not be those near the interfaces between vortices.

During mid-April 2020, a strong ridge set in the northeastern Pacific accompanied downstream over northern North America by a similarly strong trough; The strong trough developed vertically resulting in a close circulation in the middle and lower stratosphere. This ridge, in turn, extended vertically to the middle stratosphere. The pattern continued a downstream development, in which wave-activity flux pointed downward. Our results for the connections generally support those in previous works on stratospheric influences on the variability of the troposphere.

Acknowledgments

Support was provided by the U.S. NSF Grant AGS-1832842. J.C. also acknowledges the support of the RyC project RYC2018-025169.

Data Availability Statement: The data sets used here are publicly available: ERA5, Copernicus Climate Change Service (C3S) operated by ECMWF on behalf of the European Commission. DOI: 10.24381/cds.bd0915c6. They were obtained from `https://cds.climate.copernicus.eu/cdsapp#!/dataset/reanalysis-era5-pressure-levels?tab=form` [registration required]

References

Bernhard, G. H., Fioletov, V. E., Groo, J.-U., Ialongo, I., Johnsen, B., Lakkala, K., ... Svendby, T. (2020). Record-breaking increases in arctic solar ultraviolet radiation caused by exceptionally large ozone depletion in 2020. *Geophysical Research Letters*, *47*(24), e2020GL090844.

Curbelo, J., García-Garrido, V. J., Mechoso, C. R., Mancho, A. M., Wiggins, S., & Niang, C. (2017). Insights into the three-dimensional lagrangian geometry of the antarctic polar vortex. *Nonlinear Processes in Geophysics*, *24*(3), 379–392.

Curbelo, J., Mechoso, C., Mancho, A. M., & Wiggins, S. (2019a). Lagrangian study of the final warming in the southern stratosphere during 2002: Part II. 3D structure. *Climate Dynamics*, *53*(3-4), 1277–1286.

Curbelo, J., Mechoso, C., Mancho, A. M., & Wiggins, S. (2019b). Lagrangian study of the final warming in the southern stratosphere during 2002: Part I. the vortex splitting at upper levels. *Climate Dynamics*, *53*(5-6), 2779–2792.

García-Garrido, V. J., Curbelo, J., Mechoso, C. R., Mancho, A. M., & Wiggins, S. (2017). A simple kinematic model for the lagrangian description of relevant nonlinear processes in the stratospheric polar vortex. *Nonlinear Processes in Geophysics*, *24*(2), 265–278.

Guan, W., Jiang, X., Ren, X., Chen, G., Lin, P., & Lin, H. (2020). The leading intraseasonal variability mode of wintertime surface air temperature over the north american sector. *Journal of Climate*, *33*(21), 9287–9306.

Hardiman, S. C., Dunstone, N. J., Scaife, A. A., Smith, D. M., Knight, J. R., Davies, P., ...

Greatbatch, R. J. (2020). Predictability of european winter 2019/20: Indian ocean dipole impacts on the nao. *Atmospheric Science Letters*, *21*(12), e1005.

Hersbach, H., Bell, B., Berrisford, P., Biavati, G., Hornyi, A., Muoz Sabater, J., ... Thpaut, J.-N. (2018). ERA5 hourly data on pressure levels from 1979 to present. *Copernicus Climate Change Service (C3S) Climate Data Store (CDS). (Accessed on 10-Nov-2020)*. Retrieved from 10.24381/cds.bd0915c6

Kretschmer, M., Cohen, J., Matthias, V., Runge, J., & Coumou, D. (2018). The different stratospheric influence on cold-extremes in eurasia and north america. *npj Clim Atmos Sci*, *1*(44).

Lawrence, Z. D., Perlwitz, J., Butler, A. H., Manney, G. L., Newman, P. A., Lee, S. H., & Nash, E. R. (2020). The remarkably strong arctic stratospheric polar vortex of winter 2020: Links to record-breaking arctic oscillation and ozone loss. *Journal of Geophysical Research: Atmospheres*, *125*(22), e2020JD033271.

Lee, S. H., Lawrence, Z. D., Butler, A. H., & Karpechko, A. Y. (2020). Seasonal forecasts of the exceptional northern hemisphere winter of 2020. *Geophysical Research Letters*, *47*(21), e2020GL090328.

Mancho, A. M., Wiggins, S., Curbelo, J., & Mendoza, C. (2013). Lagrangian descriptors: A method for revealing phase space structures of general time dependent dynamical systems. *Communications in Nonlinear Science and Numerical Simulations*, *18*(12), 3530-3557.

Manney, G. L., & Lawrence, Z. D. (2016). The major stratospheric final warming in 2016: Dispersal of vortex air and termination of Arctic chemical ozone loss. *Atmospheric Chemistry and Physics Discussions*, *2016*, 1–40.

Manney, G. L., Lawrence, Z. D., Santee, M. L., Livesey, N. J., Lambert, A., & Pitts, M. C. (2015). Polar processing in a split vortex: Arctic ozone loss in early winter 2012/2013. *Atmospheric Chemistry and Physics*, *15*(10), 5381–5403. Retrieved from https://acp.copernicus.org/articles/15/5381/2015/ doi: 10.5194/acp-15-5381-2015

Manney, G. L., Livesey, N. J., Santee, M. L., Froidevaux, L., Lambert, A., Lawrence, Z. D., ... Fuller, R. A. (2020). Record-low arctic stratospheric ozone in 2020: Mls observations of chemical processes and comparisons with previous extreme winters. *Geophysical Research Letters*, *47*(16), e2020GL089063. doi: https://doi.org/10.1029/2020GL089063

Mariotti, A., Mechoso, C. R., Legras, B., & Daniel, V. (2000). The Evolution of the Ozone Collar in the Antarctic Lower Stratosphere during Early August 1994. *Journal of the Atmospheric Sciences*, *57*(3), 402-414.

Plumb, R. A. (1985). On the Three-Dimensional Propagation of Stationary Waves. *Journal of the Atmospheric Sciences*, *42*(3), 217-229.

Wohltmann, I., von der Gathen, P., Lehmann, R., Maturilli, M., Deckelmann, H., Manney, G. L., ... Rex, M. (2020). Near-complete local reduction of arctic stratospheric ozone by severe chemical loss in spring 2020. *Geophysical Research Letters*, *47*(20), e2020GL089547. doi: https://doi.org/10.1029/2020GL089547